Supporting Information

Boosting the in-plane thermal conductivity of nanofibrillated cellulose films: alignment engineering of cross-linked AlN whiskers

Mengyang Niu[a,#], Zheng Zhao[a,#], Baokai Wang[a], Chang Yu[a], Mengyi Li[a], Jiajun Hu [b], Lifeng Zhu [a,*], Xu Hao[a], Shiqin Wan[a], Ming Yue[c], Weiwei Xuan[d], Qipeng Lu[a], Wenbin Cao[a,*], Kexin Chen[e,*] , Qi Wang[a,*]

[a] *School of Materials Science and Engineering, University of Science and Technology Beijing, Beijing 100083, China*

[b] *State Key Laboratory for Mechanical Behavior of Materials, Xi'an Jiaotong University, Xi'an, 710049, China.*

[c] *School of Civil and Resource Engineering, University of Science and Technology Beijing, Beijing 100083, China*

[d] *School of Energy and Environmental Engineering, University of Science and Technology Beijing, Beijing 100083, China*

[e] *State Key Laboratory for Advanced Metals and Materials, University of Science and Technology Beijing, Beijing, 100083, China*

[#] Mengyang Niu and Zheng Zhao contributed equally to this work.

[*]Corresponding authors: zhu@ustb.edu.cn (L. Zhu), wbcao@ustb.edu.cn (W. Cao), kxchen@ustb.edu.cn (K. Chen), wangqi15@ustb.edu.cn (Q. Wang)

Table S1. Correspondence between mass fractions and volume fractions of AlNw in the composites.

Sample	Mass fraction of AlNw (wt%)	Volume fraction of AlNw (vol%)
NFC/AlNw-20	20	10.2
NFC/AlNw-40	40	23.2
NFC/AlNw-60	60	40.5
NFC/AlNw-70	70	51.4

Figure S1. Digital photographs of AlNw grown in the crucible.

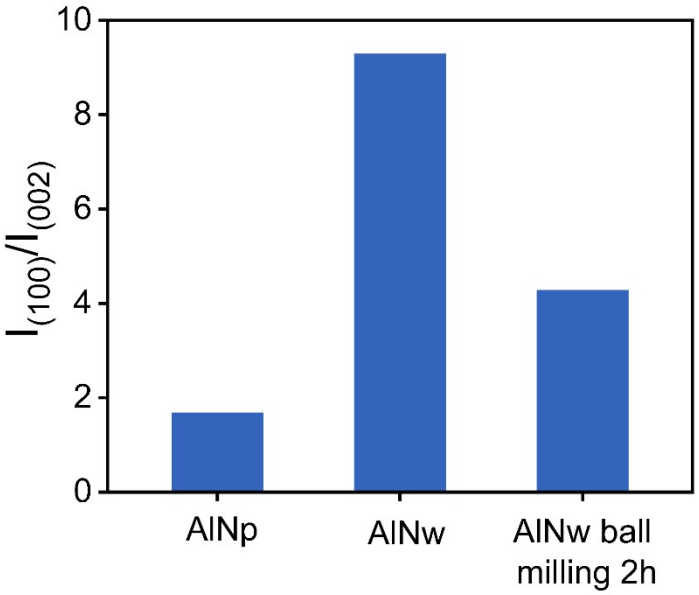

Figure S2. The $I_{(100)}/I_{(002)}$ of AlNp, as-synthesized AlNw and AlNw after ball milling.

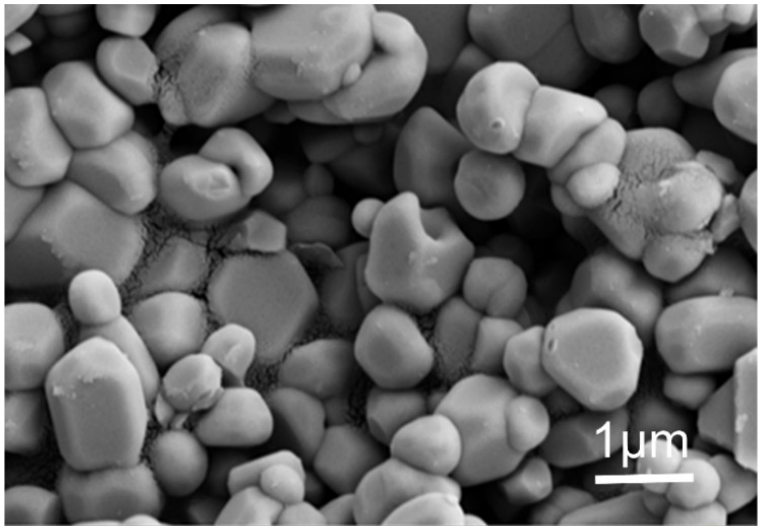

Figure S3. SEM image of commercial AlNp.

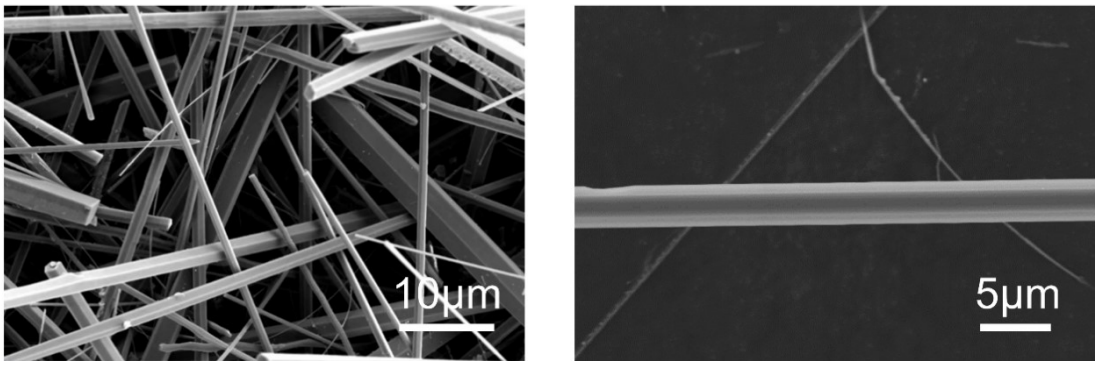

Figure S4. SEM image of AlNw with different magnifications.

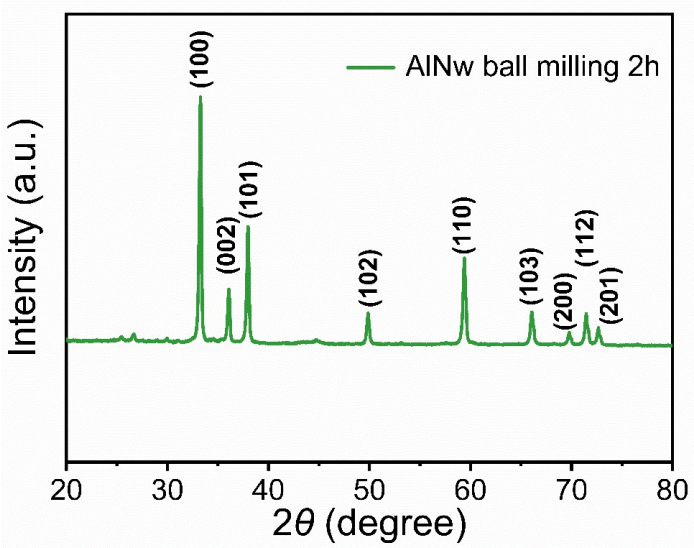

Figure S5. XRD pattern of AlNw after ball-milling.

Figure S6. The macroscopic morphology of pure NFC film.

Table S2. XRD information of NFC/ AlNw -*x* composite films

Sample	$I_{(100)}$	$I_{(002)}$	$I_{(100)}/I_{(002)}$
NFC/AlNw-20	12810	1037	12.4
NFC/AlNw-40	10264	838	12.2
NFC/AlNw-60	9442	916	10.3
NFC/AlNw-70	8384	971	8.6

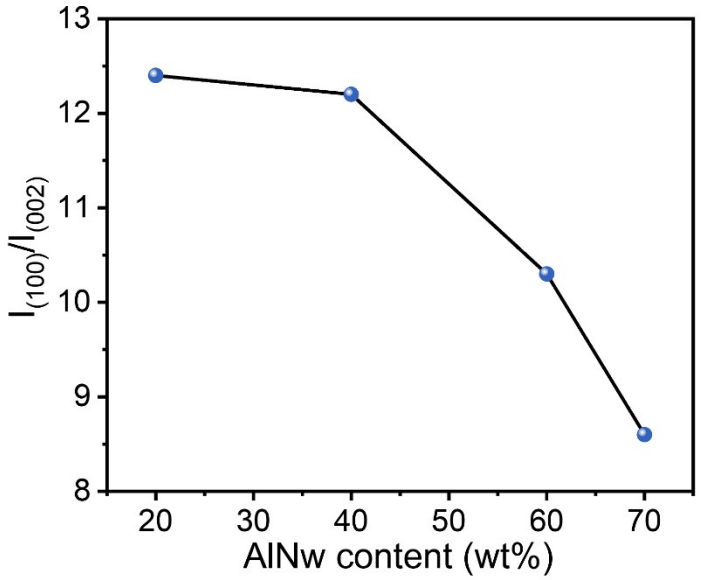

Figure S7. The $I_{(100)}/I_{(002)}$ of NFC/AlNw-*x* composite films.

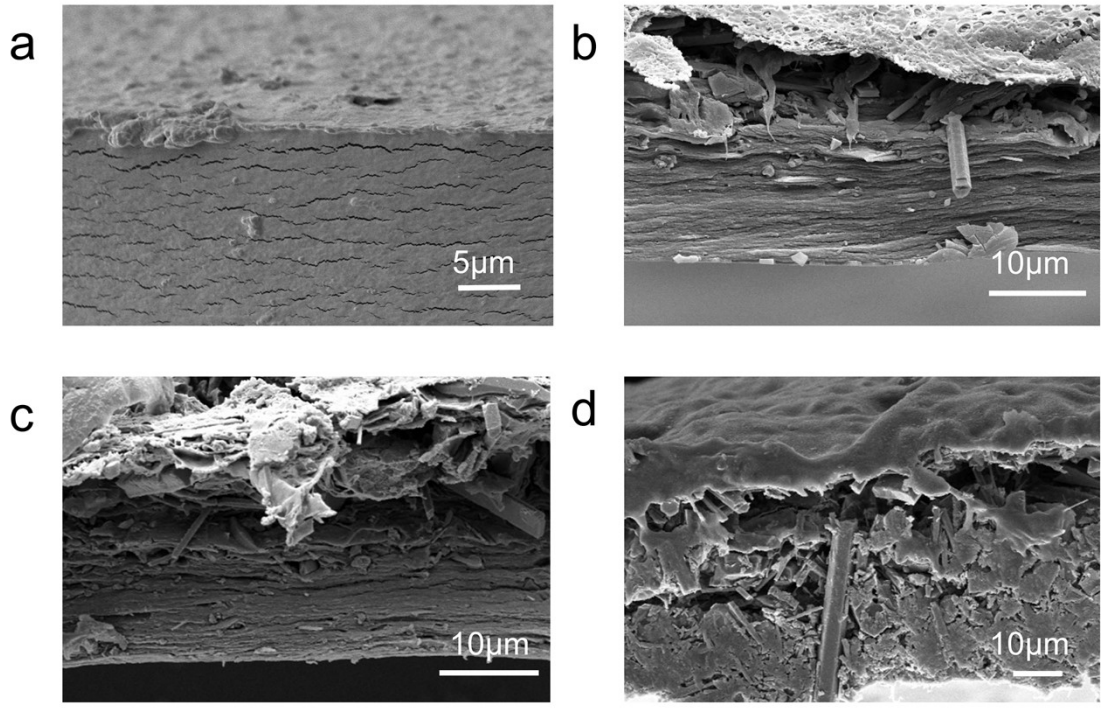

Figure S8. The cross-sectional SEM images of the NFC films with different filling fraction: (a) pure NFC; (b) NFC/AlNw-20; (c) NFC/AlNw-40; (d) NFC/AlNw-60.

Simulation process of the interface thermal resistance between AlNw and NFC matrix by the EMA model

According to the EMA model, the in-plane thermal conductivity can be calculated using the following equation[1, 2]:

$$\lambda = \lambda_{11} = \lambda_{22} = \lambda_m \left\{ \frac{2 + V_f \left[\frac{\lambda_p}{\lambda_m} \left(1 + \left\langle \cos^2 \theta \right\rangle \right) \right]}{2 - V_f \left[\frac{\lambda_p d - \lambda_m d - R_{c1} \lambda_p \lambda_m}{\lambda_p d} \left(1 - \left\langle \cos^2 \theta \right\rangle \right) \right]} \right\} \quad (1)$$

where λ_{11} and λ_{22} referred to the thermal conductivities of the composite film in different in-plane directions, λ_m and λ_p was the thermal conductivity of the polymer matrix and the filler, respectively; V_f was the volume fraction of the filler, d was the diameter of the filler, θ was the angle between the axis of symmetry at a local position within the composites and the direction perpendicular to the plane, and R_{c1} represented the interfacial thermal resistance between the filler and the matrix. For the NFC/AlNw composite film, λ_m was taken as 1.63 $W \cdot m^{-1} \cdot K^{-1}$, λ_p was taken as the theoretical value of AlN thermal conductivity (320 $W \cdot m^{-1} \cdot K^{-1}$), and d was set to 2 μm. The average value of θ was calculated by selecting over 10 AlNw in the SEM image of the composite film cross-section. In equation (1), all the parameters are known except for R_{c1}. By varying the value of R_{c1}, the thermal conductivity λ of the composite film was calculated and fitted with experimental data.

Simulation process of the interface thermal resistance between AlNw using Foygel model

In order to calculate the interfacial thermal resistance (R_{c2}) between AlNw, we introduced the Foygel model. This model was defined as follows[3, 4]:

$$K(V_f, p) = K_0(V_f - V_c)^{t(p)} \tag{2}$$

$$V_c(p > 1) \approx \frac{0.60}{p} \tag{3}$$

where K_0 represented the prefactor contribution of the thermal conductivity from the individual AlNw filler network, V_f was the volume fraction of the filler, V_c was the critical volume fraction of the filler at the thermal percolation threshold, obtained from equation (3); p represented the aspect ratio of AlNw ($p = L/d$), where L was the length of AlNw (~94.97 μm) and d was set to 2 μm. $t(p)$ denoted the thermal conductivity exponent based on the aspect ratio of AlNw. The values of K_0 and $t(p)$ were obtained by fitting the thermal conductivity (K) of the composite film using equation (2). Based on these parameters, the contact thermal resistance (R_0) between the fillers could be calculated using the following equation:

$$R_0 = (K_0 L V_c^{t(p)})^{-1} \tag{4}$$

The calculated value of R_0 was 1.10×10^3 K/W, and the average contact area between adjacent AlNw fibers could be calculated using the following equation:

$$\overline{A_s} = \frac{2D^2}{\pi}\delta(p) \tag{5}$$

$$\delta(p) = \ln\left(\frac{\sqrt{1+p^{-1}} + \sqrt{1-p^{-1}}}{\sqrt{1+p^{-1}} - \sqrt{1-p^{-1}}}\right) \tag{6}$$

By using equations (5) and (6), we obtained a value of $\bar{A}_s$ was 1.17 × 10^{-11} m^2. Consequently, the interfacial thermal resistance between AlNw (R_{c2}) was calculated as 1.29 × 10^{-8} m^2K/W.

Table S3. Comparison of in-plane thermal conductivity between NFC/AlNw composite film and some previously reported composite films.

Composites	Loading(wt%)	$\lambda_{//}$(W/(m·K))	References
NFC/AlN	25.0	4.20	5
PVA/ND@PDA	10.0	5.86	6
NFC/MgO@rGO	20.0	7.45	7
PVA/SiCNWs	50.0	14.1	8
CNC/BNNTS	20.0	13.33	9
PVA/NF-BNNS	94.0	6.90	10
NFC/MBP	15.0	17.60	11
PVA/FGN	80.0	21.60	12
PVA/MWCNT-BN	20.0	11.49	13
CNF/H-MoS_2@SiCNWs	40.0	19.76	14
PVA/Si_3N_4NWs	50.0	15.40	15
PVA/rGO	5.0	4.00	16
PMlA/AlN	50.0	17.30	17
NFC/AlNw	20.0	18.04	This work
NFC/AlNw	70.0	22.78	This work

Heat transfer simulation process for pure NFC, NFC/AlNp, and NFC/AlNw models

Finite element simulations was carried out to simulate the heat transfer processes of three typical models, that was pure NFC, NFC/AlNp, and NFC/AlNw films, using the COMSOL Multiphysics 5.4 software. For ease of setting the heat source surface, we modeled the NFC matrix as a cylindrical ring with an inner diameter of 10 μm, an outer diameter of 100 μm, and a thickness of 10 μm. In the model of the NFC/AlN spheres composite film, AlN spheres were approximated as spherical particles with a diameter of 1 μm. A total of 156 AlN spheres particles were randomly distributed within the matrix. In the model of the NFC/AlN whiskers composite film, AlN whiskers were approximated as rod-shaped structures with a length of 30 μm and a diameter of 1 μm. A total of 28 rods were arranged in the in-plane direction of the NFC matrix, ensuring that the total volume of AlN whiskers was equivalent to that of AlN spheres. The material properties were selected from the built-in material library of the software. The initial temperature of the inner surface of the cylindrical ring was set to 373.15 K as the heat source, while the initial temperatures of the remaining regions were set to room temperature, 293.15 K. Transient temperature distributions of the three models were computed and simulated.

References

1 Q. Li, Y. Guo, W. Li, S. Qiu, C. Zhu, X. Wei, M. Chen, C. Liu, S. Liao, Y. Gong, A. K. Mishra and L. Liu, *Chem. Mater.*, 2014, **26**, 4459-4465.

2 C.-W. Nan, R. Birringer, D. R. Clarke and H. Gleiter, *J. Appl. Phys.*, 1997, **81**, 6692-6699.

3 M. Foygel, R. D. Morris, D. Anez, S. French and V. L. Sobolev, *Phys. Rev. B*, 2005, **71**, 4201.

4 Y. Zhang, C. Lei, K. Wu and Q. Fu, *Adv. Sci.*, 2021, **8**, e2004821.

5 K. Zhang, P. Tao, Y. Zhang, X. Liao and S. Nie, *Carbohydr. Polym.*, 2019, **213**, 228-235.

6 B. Nan, K. Wu, W. Chen, Y. Liu, Q. Zhang and M. Lu, *Appl. Surf. Sci.*, 2020, **508**, 144797.

7 M. Ma, L. Xu, L. Qiao, S. Chen, Y. Shi, H. He and X. Wang, *Chem. Eng. J.*, 2020, **392**, 123714.

8 Z. Chen, S. Gao, J. Zhang, D. Liu, J. Zeng, Y. Yao, J.-B. Xu and R. Sun, *Compos. Commun.*, 2023, **41**, 101654.

9 Q. He, L. Ding, L. Wu, Z. Zhou, Y. Wang, T. Xu, N. Wang, K. Zhang, X. Wang, F. Ding, J. Zhang and Y. Yao, *Small Struct.*, 2023, **4**, 2200282.

10 Z. Xiaoliang, Y. Lei, Y. Shuhui, L. Hao, S. Rong, X. Jianbin and W. Ching-Ping, *Nanoscale*, 2015, **7**, 6774-6781.

11 J. Hu, H. Xia, X. Hou, T. Yang, K. Si, Y. Wang, L. Wang and Z. Shi, *J. Mater. Chem. A*, 2021, **9**, 27049-27060.

12 X. Chen, M. Wang, J. Cheng, C. Zhao and Z. Tang, *Mater. Today Chem.*, 2023, **29**, 101422.

13 J. Zhou, Z. Yu, Y. Lv, C. Wang, P. Hu and Y. Liu, *Compos. Pt. A-Appl. Sci. Manuf.*, 2022, **163**, 107195.

14 B. Xue, S. Yang, X. Sun, L. Xie, S. Qin and Q. Zheng, *J. Mater. Chem. A*, 2020, **8**, 14506-14518.

15 S. Wan, X. Hao, L. Zhu, C. Yu, M. Li, Z. Zhao, J. Kuang, M. Yue, Q. Lu, W. Cao and Q. Wang, *ACS Appl. Mater. Interfaces*, 2023, **15**, 32885-32894.

16 F. Luo, M. Zhang, S. Chen, J. Xu, C. Ma and G. Chen, *Compos. Sci. Technol.*, 2021, **207**, 108707.

17 H. Ruan, F. Lü, J. Song, X. Bian, K. Yin, S. Yin and Q. Xie, *Compos. Sci. Technol.*, 2022, **224**, 109477.